Measurement of the transverse single-spin asymmetry for forward neutron production in a wide p_T range in polarized $p+p$ collisions at $\sqrt{s}=510$ GeV

M. H. Kim,[1] O. Adriani,[2,3] E. Berti,[2,3] L. Bonechi,[3] R. D'Alessandro,[2,3] Y. Goto,[1,4] B. Hong,[5] Y. Itow,[6,7] K. Kasahara,[8] Y. Kim,[9] J. H. Lee,[10] S. H. Lee,[9] T. Ljubicic,[10] H. Menjo,[6] G. Mitsuka,[11] I. Nakagawa,[1,4] A. Ogawa,[10] S. Oh,[9] T. Sako,[12] N. Sakurai,[13] K. Sato,[6] R. Seidl,[1,4] K. Tanida,[14] S. Torii,[15] and A. Tricomi[16,17,18]

(RHICf Collaboration)

[1]*RIKEN Nishina Center for Accelerator-Based Science, Wako, Saitama 351-0198, Japan*
[2]*Department of Physics and Astronomy, University of Florence, Sesto Florentino I-50019, Italy*
[3]*INFN Section of Florence, Sesto Florentino I-50019, Italy*
[4]*RIKEN BNL Research Center, Brookhaven National Laboratory, Upton, 11973-5000 New York, USA*
[5]*Korea University, Seoul 02841, Korea*
[6]*Institute for Space-Earth Environmental Research, Nagoya University, Nagoya 464-8602, Aichi, Japan*
[7]*Kobayashi-Maskawa Institute for the Origin of Particles and the Universe, Nagoya University, Nagoya 464-8602, Aichi, Japan*
[8]*Shibaura Institute of Technology, Minuma-ku, 337-8570 Saitama, Japan*
[9]*Sejong University, Seoul 05000, Korea*
[10]*Brookhaven National Laboratory, Upton, 11973-5000 New York, USA*
[11]*KEK, High Energy Accelerator Research Organization, Tsukuba, Ibaraki 305-0801, Japan*
[12]*Institute for Cosmic Ray Research, University of Tokyo, Kashiwa, 277-8582 Chiba, Japan*
[13]*Tokushima University, 770-8051, Tokushima, Japan*
[14]*Advanced Science Research Center, Japan Atomic Energy Agency, 2-4 Shirakata Shirane, Tokai-mura, Naka-gun, Ibaraki-ken 319-1195, Japan*
[15]*RISE, Waseda University, Shinjuku, 162-0044 Tokyo, Japan*
[16]*Department of Physics and Astronomy, University of Catania, Catania I-95123, Italy*
[17]*INFN Section of Catania, Catania I-95123, Italy*
[18]*CSFNSM, Catania I-95123, Italy*

(Received 15 October 2023; accepted 4 December 2023; published 5 January 2024)

Transverse single-spin asymmetries A_N of forward neutrons at pseudorapidities larger than 6 had only been studied in the transverse momentum range of $p_T < 0.4$ GeV/c. The RHICf Collaboration has extended the previous measurements up to 1.0 GeV/c in polarized $p+p$ collisions at $\sqrt{s}=510$ GeV, using an electromagnetic calorimeter installed in the zero-degree area of the STAR detector at the Relativistic Heavy Ion Collider. The resulting A_N values increase in magnitude with p_T in the high longitudinal momentum fraction x_F range, but they reach a plateau at lower p_T for lower x_F values. For low transverse momenta, the A_N's show little x_F dependence and level off from intermediate values. For higher transverse momenta, the A_N's also show a tendency to reach a plateau at increased magnitudes. The results are consistent with previous measurements at lower collision energies, suggesting no $\sqrt{s}$ dependence of the neutron asymmetries. A theoretical model based on the interference of π and a_1 exchange between two protons could partially reproduce the current results; however, an additional mechanism is necessary to describe the neutron A_N's over the whole kinematic region measured.

DOI: 10.1103/PhysRevD.109.012003

I. INTRODUCTION

With the discovery of a large transverse single-spin asymmetry (A_N) for forward neutron production [1] from the first polarized $p+p$ collisions at a center-of-mass energy ($\sqrt{s}$) of 200 GeV at the Relativistic Heavy Ion Collider (RHIC), the spin-dependent production mechanism of the forward neutron has attracted great interest over ten years. The discovery also inspired the PHENIX experiment to measure the neutron A_N's at $\sqrt{s}=62$ GeV, 200 GeV, and 500 GeV [2] at transverse momenta (p_T) less than 0.4 GeV/c and indicated a possible p_T dependence of the neutron A_N. The one-pion exchange (OPE) model [3–5], which successfully described the unpolarized forward neutron production [6], introduced an interference

between spin flip π and spin nonflip a_1 exchange between the two protons. This theoretical framework reproduced the PHENIX data reasonably well, showing that the neutron A_N's increased with increasing p_T, with little $\sqrt{s}$ dependence [7]. Recently, the A_N's at $\sqrt{s} = 200$ GeV in Ref. [2] were extracted as a function of the longitudinal momentum fraction (x_F) and p_T [8]. The results were consistent with the model calculations, but only relatively low transverse momenta were accessed.

The A_N value is defined by a left-right cross section asymmetry as

$$A_N = \frac{d\sigma_{\text{left}} - d\sigma_{\text{right}}}{d\sigma_{\text{left}} + d\sigma_{\text{right}}}, \tag{1}$$

where $d\sigma_{\text{left(right)}}$ is the particle-production cross section in the left (right) side of the beam polarization. A_N's of forward particle production at pseudorapidities (η) larger than 6 at the RHIC are especially important for studying the production mechanism of the particles in a region where perturbative quantum chromodynamics is not applicable. Thus far, the neutron A_N has been studied only in a narrow kinematic range in $p_T < 0.4$ GeV/c. Measurements at higher values, $p_T > 0.4$ GeV/c, have been awaited in order to study the production mechanism of forward neutrons in more detail. Here, the RHIC forward (RHICf) Collaboration has extended the kinematic range of the previous measurements up to 1.0 GeV/c with 1 order of magnitude better position and p_T resolutions not only to explicitly explore the kinematic dependence of the neutron A_N in a wider p_T and x_F range, but also to study the $\sqrt{s}$ dependence by comparing the results with those of PHENIX.

This paper is organized as follows: The experimental setup and data taking of the RHICf experiment are presented in Sec. II. The selection criteria for good events and neutron candidates are explained in Sec. III. Section IV describes the procedures of the background subtraction, unfolding, and asymmetry calculation. The results are discussed in Sec. V, and the paper is summarized in Sec. VI.

II. THE RHICf EXPERIMENT

In June 2017, the RHICf experiment measured forward neutral particles produced in $\eta > 6$ from transversely polarized $p + p$ collisions at $\sqrt{s} = 510$ GeV in the zero-degree area of the STAR detector system at the RHIC. Figure 1 shows the experimental setup of the RHICf experiment. STAR employs two zero-degree calorimeters (ZDCs) [9] located 18 m east and west from the nominal beam collision point. The former LHCf Arm1 detector [10], which will be called the RHICf detector [11] hereafter, was installed in front of the west ZDC. A thin scintillator front counter (FC) was also positioned in front of the RHICf detector to suppress the charged hadron background. The RHICf detector consists of two sampling calorimeters that

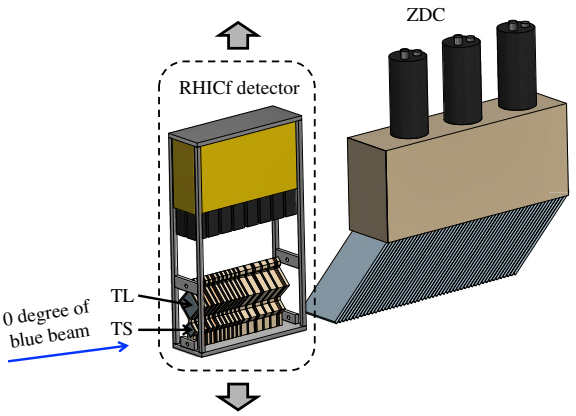

FIG. 1. Setup of the RHICf experiment. The data were taken by moving the RHICf detector to cover a wide p_T range of $0.0 < p_T < 1.0$ GeV/c.

have effective areas of 20 mm × 20 mm (small tower, TS) and 40 mm × 40 mm (large tower, TL), respectively. Both are composed of 17 layers of tungsten absorbers with 1.6 nuclear interaction lengths in total, 16 layers of GSO scintillator plates, and 4 XY hodoscope layers covered by 1-mm-wide GSO bars.

RHICf used 90°-rotated transversely polarized beams (radial to the RHIC rings) instead of the usual vertically polarized beams. Neutrons with a wide p_T range of $0.0 < p_T < 1.0$ GeV/c were measured by moving the detector vertically. We also requested a large β^* of 8 m for smaller angular beam divergence. Under these conditions, the luminosity was at the level of about 10^{31} cm^{-2} s^{-1}. See Ref. [12] for more details on the experimental conditions.

III. EVENT RECONSTRUCTION AND SELECTION

Before presenting the analysis selection criteria, the neutron and photon events are defined as follows: A neutron event is defined as an event in which a neutron is produced by a collision and is directed toward the detector. When there is no neutron, a photon event is defined as an event in which at least one photon hits the detector. The neutron events are mainly measured by the shower trigger that is activated when the energy deposits of any three consecutive GSO plates are larger than 45 MeV. Since the shower trigger is sensitive not only to the neutron events but also to the photon events, the neutron candidates are identified by using the variable L_{2D}, defined by

$$L_{2D} = L_{90\%} - 0.15 L_{20\%}, \tag{2}$$

where $L_{x\%}$ is defined by the longitudinal depth for the measured integrated energy deposition in the GSO plates to reach $x\%$ of the total in units of the radiation length (X_0). While neutrons mainly generate the hadronic showers in deeper layers of the RHICf detector and do not necessarily deposit all their energy in the detector, photons generate the

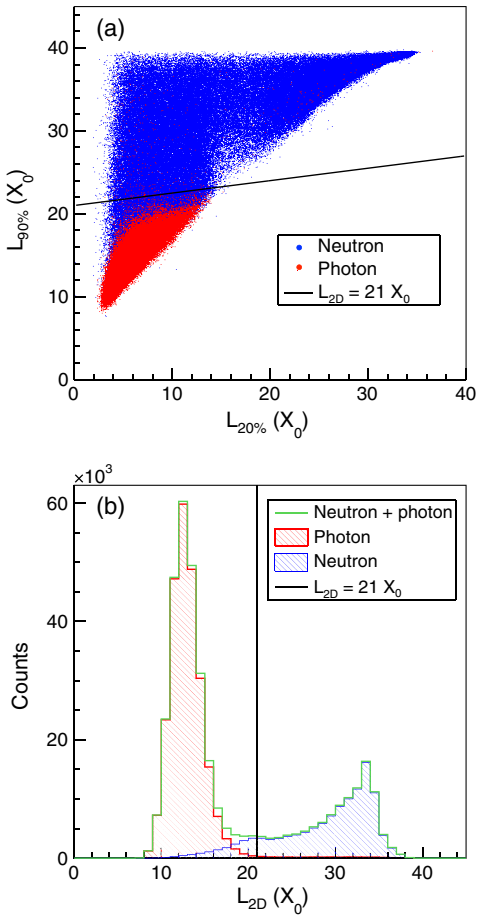

FIG. 2. (a) $L_{90\%}$ versus $L_{20\%}$ and (b) L_{2D} distributions of neutron and photon events in the QGSJET II-04 sample. The black lines correspond to the threshold to select a neutron candidate, which is $L_{2D} = 21X_0$.

electromagnetic shower in shallow layers and deposit all their energy. Figures 2(a) and 2(b) show the $L_{90\%}$ versus $L_{20\%}$ and L_{2D} distributions of the neutron and photon events, respectively, in a Monte Carlo (MC) sample, where the $p + p$ collisions were generated by QGSJET II-04 [13]. An event is identified as a neutron if the L_{2D} was larger than 21 X_0. This threshold was optimized by taking into account the neutron purity and efficiency, which were estimated by a GEANT4 [14] simulation with the QGSP_BERT4.0 model.

Hit positions of the neutrons were calculated by fitting the energy deposit distribution in the GSO bars using a Lorentzian-based function. One of the four hodoscope layers with the maximum energy deposition was used for the position determination. The energies of the neutrons were reconstructed using a relation between the energy deposit sum of the GSO plates and the incident energy of neutrons obtained by GEANT4 simulations. The position-dependent light collection efficiency and shower lateral leakage effect were also corrected in the simulation. Although the energy range was different, the above reconstructions were also applied for the previous analyses [10,15] that used the RHICf detector. See Refs. [11,16,17] for more details on the reconstruction and correction procedures.

In order to study the detector performance for neutron reconstruction, 10^5 neutrons were generated at the center of the detector in the GEANT4 simulation, and their positions and energies were reconstructed in the same way as for the data. For 200 GeV neutrons, the energy and position resolutions of the RHICf detector were 37% and 1.1 mm, respectively. To improve the energy resolution, hadronic showers that developed deeper into the RHICf detector were excluded by requiring $L_{90\%} < 37X_0$. This condition improved the energy resolution of neutrons at, e.g., 200 GeV, from 37% to 30%. The RHICf detector was located downstream of a RHIC dipole magnet, DX. Neutron candidate hits were rejected if they overlapped with the shadow of the DX magnet, or if their distance to the detector edge was smaller than 2 mm, because of the poor performance in these regions. In principle, only neutral particles can reach the detector from the collision point, because the DX magnet sweeps away charged particles. However, the detector can detect charged particles when neutral hadrons hit the DX magnet and create a hadronic shower. Events with ADC values of the FC larger than 25% of the minimum ionizing particle (MIP) peak position were excluded to suppress the charged hadron background.

IV. BACKGROUND SUBTRACTION AND UNFOLDING

In the RHIC ring, the beam circulating clockwise is called the "blue beam," and the one circulating counterclockwise is called the "yellow beam." Since the RHICf detector was installed in the direction where the blue beam heads, only the blue beam polarization was considered for the forward A_N measurements. On the other hand, when the backward A_N was measured, only the yellow beam polarization was taken into account. Since RHICf used the beam polarization, which was normal to the detector motion, as shown in Fig. 1, the tower that was off-center of the beam measured only a narrow azimuthal range of $\sigma_{\text{left(right)}}$ when the beam polarization was up (down). In such a case, the A_N was defined by

$$A_N = \frac{1}{PD_\phi}\left(\frac{N^\uparrow - RN^\downarrow}{N^\uparrow + RN^\downarrow}\right), \tag{3}$$

where P is the beam polarization, ranging from 0.54 to 0.61 for the blue beam and from 0.53 to 0.61 for the yellow beam, and $N^{\uparrow(\downarrow)}$ is the number of neutrons detected when the beam polarization is up (down). The beam polarization was measured by carbon target polarimeters [18] and normalized by the absolute polarization measured by a hydrogen jet polarimeter [19]. Systematic uncertainties of the blue and yellow beam polarizations were 3.7%

and 3.4%, respectively. R, estimated by the charged particle rates from the STAR's beam beam counter [20] and vertex position detector [21], is the ratio of luminosities with the polarization of the blue beams up and down, and ranged from 0.958 to 0.995. D_ϕ is a dilution factor estimated by

$$D_\phi = \frac{1}{N}\sum_i \sin\phi_i, \tag{4}$$

where ϕ_i is the azimuthal angle of a neutron with respect to the beam polarization in the ith event and N is the number of total detected neutrons. D_ϕ was used to compensate the dilution of A_N originated from a finite ϕ distribution of neutrons. The average value of D_ϕ was 0.977. If the neutron was measured by the tower on the beam center, the azimuthal angles were divided into eight equidistant bins, and the azimuthal modulation of the A_N was measured by

$$A_N(\phi) = \frac{1}{P}\left(\frac{\sqrt{N_\phi^\uparrow N_{\phi+\pi}^\downarrow} - \sqrt{N_{\phi+\pi}^\uparrow N_\phi^\downarrow}}{\sqrt{N_\phi^\uparrow N_{\phi+\pi}^\downarrow} + \sqrt{N_{\phi+\pi}^\uparrow N_\phi^\downarrow}}\right), \tag{5}$$

where $N_{\phi(\phi+\pi)}^{\uparrow(\downarrow)}$ is the number of neutrons detected in an azimuthal angular bin $\phi(\phi+\pi)$ when the blue beam polarization is up (down). The A_N was then calculated by fitting the azimuthal modulation with a sine function where magnitude and phase were left as free parameters.

In order to study the kinematic dependence of the neutron A_N, the x_F and p_T values were divided into equidistant intervals of 0.1 and 0.05 GeV/c, respectively. Due to the finite position and energy resolutions of the detector, kinematic values of the neutrons were unfolded, but the background contaminations in the neutron candidates were subtracted first before unfolding. Two background sources for the photon and charged hadron events were considered. The contaminations in the two background event samples were subtracted for the up and down polarization cases separately:

$$N_{\text{neu}}^\uparrow = N_{\text{trig}}^\uparrow - N_{\text{pho}}^\uparrow - N_{\text{cha}}^\uparrow, \tag{6}$$

$$N_{\text{neu}}^\downarrow = N_{\text{trig}}^\downarrow - N_{\text{pho}}^\downarrow - N_{\text{cha}}^\downarrow, \tag{7}$$

where $N_{\text{trig}}^{\uparrow(\downarrow)}$, $N_{\text{neu}}^{\uparrow(\downarrow)}$, $N_{\text{pho}}^{\uparrow(\downarrow)}$, and $N_{\text{cha}}^{\uparrow(\downarrow)}$ are the number of triggered, neutron, photon, and charged hadron events, respectively, when the blue beam polarization is up (down). The charged hadron events are defined as at least one charged hadron hitting the detector when there is no neutron produced by the collision that heads toward the detector. In order to estimate the values of $N_{\text{pho}}^\uparrow$ and $N_{\text{pho}}^\downarrow$, we performed a template fit of the L_{2D} distribution by scaling the neutron and photon events of the same kinematic bin in the QGSJET II-04 sample separately. Figure 3 shows an example of the template fit for one kinematic bin. The down-to-up ratios of the neutron and photon events, $N_{\text{neu}}^\downarrow/N_{\text{neu}}^\uparrow$ and $N_{\text{pho}}^\downarrow/N_{\text{pho}}^\uparrow$, in Fig. 3, estimated by the scaled templates, are 1.077 ± 0.014 and 0.920 ± 0.012, which is consistent with the sign of the previously measured neutron [1,2] and π^0 asymmetries [12]. Figure 4 shows the A_N's of the neutron and photon events calculated using the template fits and enhanced samples before unfolding. The neutron and photon enhanced samples were selected by applying $L_{2D} > 21X_0$ and $L_{90\%} < 18X_0$ [12], respectively. Consistencies between the two A_N's calculated by the above two methods prove that the numbers of neutrons and photons were correctly estimated by the template fit. The photon contamination estimated by the template fit, which was less than 0.7% of the total neutron candidate sample, was subtracted. In Fig. 3, The larger L_{2D} values of data in $15 < L_{2D} < 21X_0$ indicate that the photon energy distribution of data is higher than that of MC because photons with higher energy generally deposit

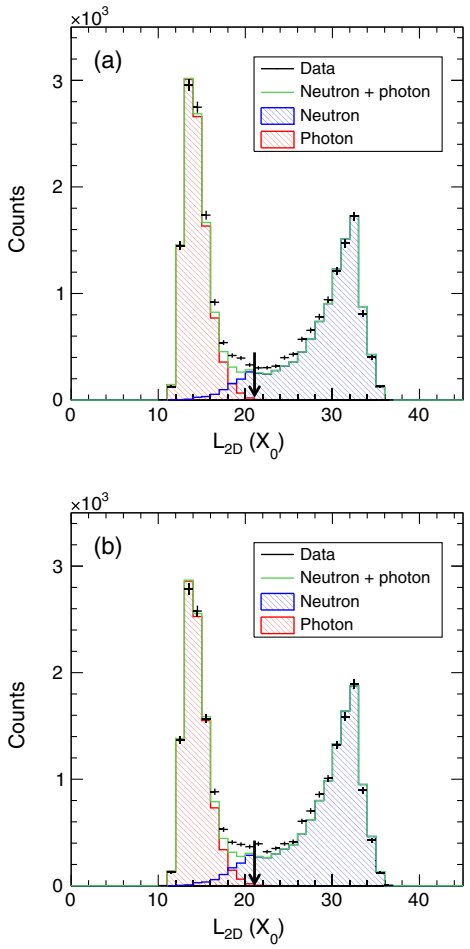

FIG. 3. Template fit of the L_{2D} distribution for the events where the blue beam spin orientation is (a) up and (b) down. The arrows show the threshold for selecting the neutron candidates, which is $L_{2D} = 21X_0$. The kinematic range of the L_{2D} distribution is $0.50 < x_F < 0.60$ and $0.30 < p_T < 0.35$ GeV/c.

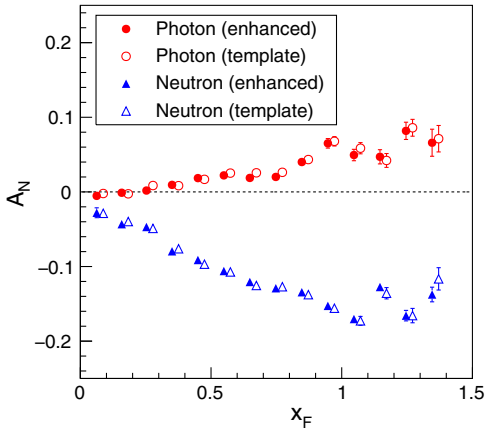

FIG. 4. The neutron and photon A_N's calculated using the template fits and enhanced samples. Note that x_F is a reconstructed value that is not unfolded, and that different p_T bins were integrated. The central x_F values for the points from the template fit were shifted for better visibility.

energy over a larger longitudinal region, making the L_{2D} value larger than for lower-energy photons. To study the effect of the discrepancies, the photon event template of the ith x_F bin was replaced by that of the $(i+1)$th x_F bin. The template fit was improved, but the A_N difference between the two template fits after unfolding was negligible, which was less than 0.0007. We concluded that the effect of the discrepancies was negligible; thereby, we did not consider the systematic uncertainty of the template fit.

Another template fit was performed to the ADC distribution of the FC to estimate the $N^{\uparrow}_{\mathrm{cha}}$ and $N^{\downarrow}_{\mathrm{cha}}$ by scaling the neutron and charged hadron event templates of the same kinematic bin in the QGSJET II-04 sample separately. Figure 5 shows an example of the template fit. The average contamination of charged hadron events in the neutron

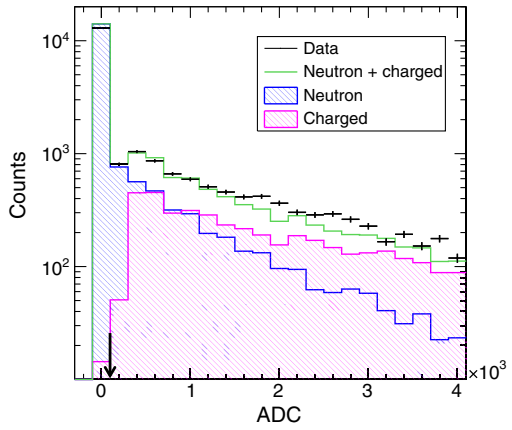

FIG. 5. Template fit of the ADC distribution of FC when the blue beam is polarized up. The arrow shows the threshold to suppress the charged hadron background, which is ADC > 0.25MIP. The kinematic range of the ADC distribution is $0.10 < x_F < 0.20$ and $0.05 < p_T < 0.10$ GeV/c.

candidate sample, which was selected by applying $L_{2D} > 21X_0$, was 0.2%, which was subtracted from the up and down polarization events separately. Since the template fit of the ADC distribution was an independent process of the one performed with the L_{2D} distribution, the following two cases were considered to study the systematic uncertainty in the charged hadron subtraction process: every charged hadron event (i) had at least one photon, or (ii) did not have any photon. In the case of (i), only the photon contamination was subtracted, because the charged hadron contamination was less than that of the photon. In the case of (ii), the two contaminations were subtracted respectively. The difference between the two cases was negligible on the A_N's, being less than 0.0004. Therefore, we also did not assign a systematic uncertainty to the process of the charged hadron subtraction. According to QGSJET II-04, the neutron candidate sample was composed 95.0% of neutrons, 3.5% of Λ's, and 1.5% of neutral kaons, after background subtraction.

The kinematic values of the neutrons, x_F, p_T, and ϕ, were unfolded using the Bayesian unfolding method [22] as implemented in the RooUnfold [23] package of ROOT [24]. For the prior, a MC sample, where the neutrons from 0 to 255 GeV were uniformly generated on the detector, was used to avoid any bias from the particular particle productions. The iterative procedure was stopped when the χ^2 change between two outputs of consecutive iterations became smaller than 1. The variation of A_N by uncertainties of the unfolded data points was considered one of the systematic uncertainties. This uncertainty is the dominating systematic uncertainty. We generated finite asymmetries by assigning up and down spin patterns in the QGSJET II-04 sample and confirmed that the unfolded spectra reproduced the input $\langle x_F \rangle$, $\langle p_T \rangle$, and A_N well within the total uncertainty that included the statistical and systematic uncertainties. The differences between the reconstructed and input $\langle x_F \rangle$ and $\langle p_T \rangle$ values were less than 0.04 and 0.02 GeV/c, respectively. Besides the systematic uncertainty of the unfolding process, the uncertainty of the beam center calculation was also considered. The beam center was measured by two methods [12], and half of the A_N difference between the two methods was assigned as systematic uncertainty.

V. RESULTS

Figure 6, Tables I, and II summarize the A_N's for forward neutron production as functions of $\langle x_F \rangle$ and $\langle p_T \rangle$ measured by the RHICf experiment. Figure 6(a) shows the neutron A_N's as a function of p_T in three different x_F ranges. In the low-x_F range, the neutron A_N reaches a plateau at low p_T. In the high-x_F range, the plateau does not seem to be reached yet, while the absolute value of the A_N explicitly increases in magnitude with p_T. Figure 6(b) shows the A_N's as a function of x_F in five different p_T ranges. The backward A_N's are all consistent with zero. In the low-p_T range

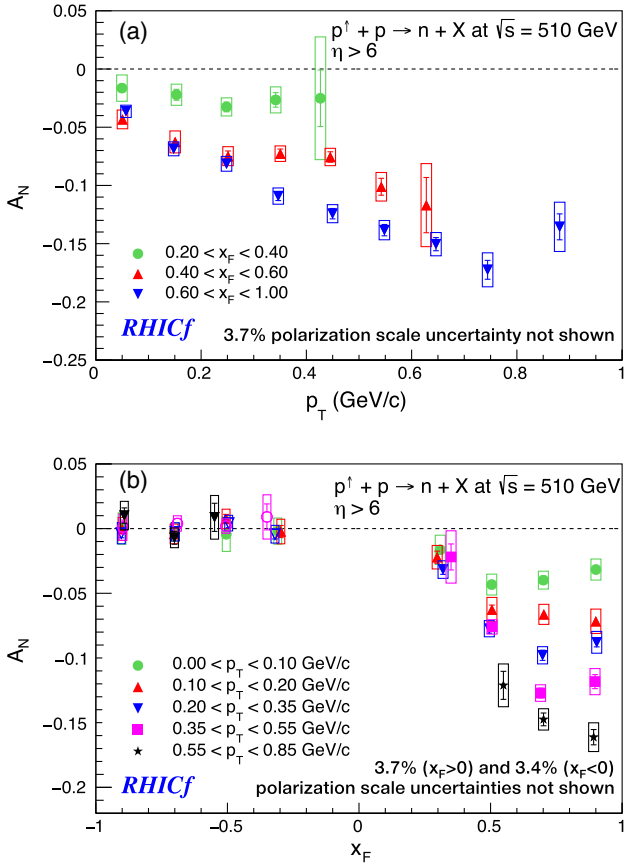

FIG. 6. A_N for forward neutron production as a function of (a) p_T and (b) x_F. Error bars correspond to the statistical uncertainties, and the boxes represent the total systematic uncertainties.

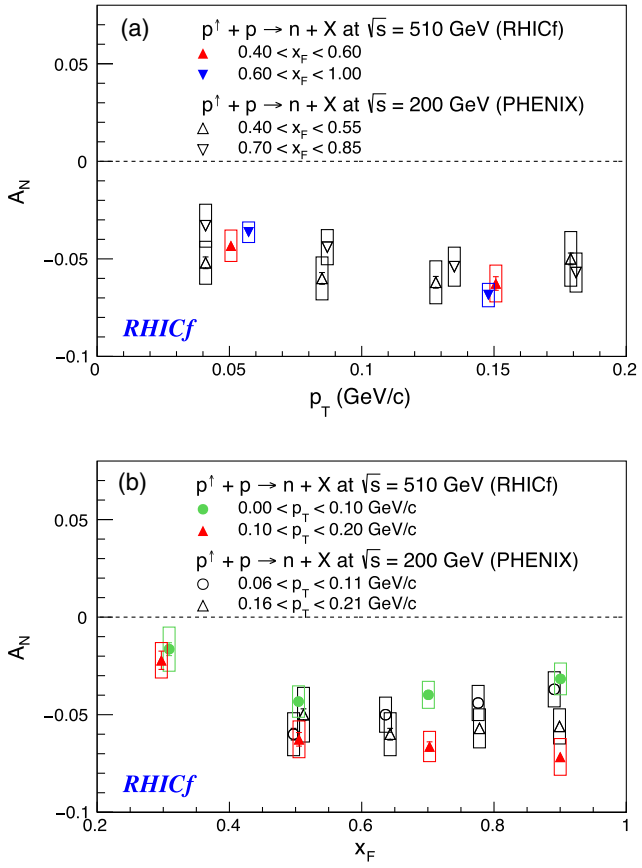

FIG. 7. Comparison of the RHICf results with those of PHENIX as functions of (a) p_T and (b) x_F.

< 0.20 GeV$/c$, the forward A_N reaches a plateau of low A_N at low x_F (about 0.5) with little x_F dependence. In the high-p_T range > 0.20 GeV$/c$, the asymmetries appear to be leveling off at higher x_F (about 0.7), showing a clear x_F dependence. The x_F dependence in the high-p_T range was observed for the first time by the RHICf experiment. Figure 7(a) shows the comparison between the RHICf and PHENIX data as a function of p_T. In the range of low $p_T < 0.2$ GeV$/c$ and $x_F > 0.4$ that is overlapping with the PHENIX data at $\sqrt{s} = 200$ GeV, the asymmetries are consistent with those by RHICf at $\sqrt{s} = 510$ GeV. Figure 7(b) shows the comparison between the two experiments as a function of x_F. In the low-p_T range that PHENIX covers at $\sqrt{s} = 200$ GeV, the asymmetries are again consistent at both energies and show a flat x_F dependence. Figures 7(a) and 7(b) suggest that there is either only a weak $\sqrt{s}$ dependence or none at all.

The RHICf data are also compared to model calculations [7] based on the π and a_1 exchange, as shown in Fig. 8. The model did not predict the x_F dependence of the neutron A_N. In the high-x_F range, the A_N's are mostly consistent with the model calculations. However, the model does not reproduce the A_N's in the low-x_F range, where the asymmetries

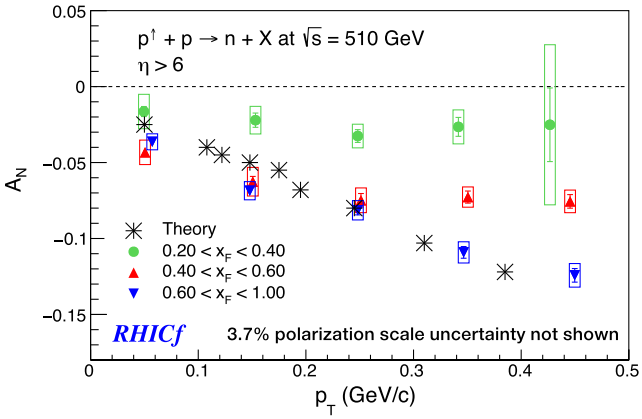

FIG. 8. Comparison of the RHICf results with the theoretical calculations.

are significantly smaller. This may be because fragmentation is expected to dominate neutron production at low x_F over Reggeon exchange.

The π and a_1 exchange model partially reproduces the current results, but it does not explain the x_F dependence. In Fig. 6(a), A_N's in $0.40 < x_F < 0.60$ and $0.60 < x_F < 1.00$ are consistent in $p_T < 0.3$ GeV$/c$, but a x_F dependence is

TABLE I. A_N's for forward neutron production as functions of $\langle x_F \rangle$ and $\langle p_T \rangle$. A_N's and kinematic values from Fig. 6(a) are listed.

				Systematic uncertainty		
$\langle x_F \rangle$	$\langle p_T \rangle$ (GeV/c)	A_N	Statistical uncertainty	Total	Beam center	Unfolding
0.30	0.04	−0.0164	0.0033	0.0112	0.0003	0.0112
0.29	0.15	−0.0221	0.0046	0.0090	0.0006	0.0089
0.31	0.24	−0.0325	0.0041	0.0077	0.0002	0.0077
0.34	0.34	−0.0262	0.0062	0.0111	0.0008	0.0109
0.34	0.42	−0.0251	0.0242	0.0526	0.0361	0.0383
0.50	0.05	−0.0432	0.0022	0.0077	0.0006	0.0077
0.50	0.15	−0.0626	0.0034	0.0087	0.0047	0.0073
0.49	0.25	−0.0748	0.0044	0.0079	0.0025	0.0075
0.49	0.35	−0.0727	0.0039	0.0065	0.0003	0.0065
0.50	0.44	−0.0755	0.0044	0.0071	0.0004	0.0071
0.54	0.54	−0.1011	0.0072	0.0118	0.0004	0.0118
0.54	0.62	−0.1169	0.0237	0.0354	0.0117	0.0334
0.80	0.05	−0.0363	0.0014	0.0051	0.0004	0.0051
0.80	0.15	−0.0685	0.0015	0.0057	0.0012	0.0056
0.79	0.24	−0.0814	0.0030	0.0060	0.0001	0.0060
0.80	0.34	−0.1091	0.0038	0.0067	0.0003	0.0067
0.74	0.44	−0.1242	0.0044	0.0071	0.0006	0.0071
0.75	0.54	−0.1383	0.0048	0.0078	0.0003	0.0078
0.76	0.64	−0.1504	0.0056	0.0095	0.0020	0.0093
0.81	0.74	−0.1724	0.0081	0.0137	0.0018	0.0136
0.88	0.88	−0.1355	0.0111	0.0200	0.0057	0.0192

TABLE II. A_N's for forward neutron production as functions of $\langle x_F \rangle$ and $\langle p_T \rangle$. A_N's and kinematic values from Fig. 6(b) are listed.

				Systematic uncertainty		
$\langle x_F \rangle$	$\langle p_T \rangle$ (GeV/c)	A_N	Statistical uncertainty	Total	Beam center	Unfolding
−0.89	0.67	0.0100	0.0059	0.0107	0.0017	0.0106
−0.70	0.64	−0.0071	0.0049	0.0075	0.0007	0.0075
−0.54	0.58	0.0087	0.0108	0.0168	0.0051	0.0160
−0.89	0.43	0.0011	0.0054	0.0099	0.0013	0.0098
−0.69	0.44	0.0039	0.0038	0.0059	0.0003	0.0059
−0.50	0.43	0.0019	0.0032	0.0053	0.0004	0.0052
−0.34	0.38	0.0090	0.0100	0.0171	0.0012	0.0170
−0.90	0.27	−0.0035	0.0035	0.0081	0.0021	0.0078
−0.69	0.26	−0.0025	0.0039	0.0066	0.0014	0.0064
−0.49	0.27	0.0042	0.0035	0.0059	0.0005	0.0059
−0.31	0.26	−0.0043	0.0036	0.0067	0.0003	0.0067
−0.90	0.15	−0.0002	0.0020	0.0090	0.0004	0.0090
−0.70	0.14	−0.0040	0.0023	0.0075	0.0012	0.0074
−0.50	0.15	0.0074	0.0034	0.0074	0.0000	0.0074
−0.29	0.15	−0.0022	0.0047	0.0090	0.0005	0.0090
−0.90	0.06	0.0000	0.0019	0.0121	0.0000	0.0121
−0.70	0.05	−0.0025	0.0019	0.0069	0.0002	0.0069
−0.50	0.05	−0.0043	0.0022	0.0126	0.0000	0.0126
−0.30	0.04	−0.0019	0.0033	0.0100	0.0000	0.0100
0.30	0.49	−0.0164	0.0033	0.0112	0.0003	0.0112
0.50	0.50	−0.0432	0.0022	0.0077	0.0006	0.0077
0.70	0.54	−0.0398	0.0019	0.0067	0.0004	0.0067
0.90	0.60	−0.0316	0.0019	0.0078	0.0011	0.0077

(Table continued)

TABLE II. *(Continued)*

				Systematic uncertainty		
$\langle x_F \rangle$	$\langle p_T \rangle$ (GeV/c)	A_N	Statistical uncertainty	Total	Beam center	Unfolding
0.29	0.15	−0.0221	0.0046	0.0090	0.0006	0.0089
0.50	0.15	−0.0626	0.0034	0.0087	0.0047	0.0073
0.70	0.14	−0.0662	0.0023	0.0074	0.0013	0.0073
0.90	0.15	−0.0716	0.0020	0.0090	0.0025	0.0087
0.31	0.26	−0.0316	0.0036	0.0067	0.0001	0.0067
0.49	0.27	−0.0773	0.0035	0.0059	0.0010	0.0058
0.69	0.26	−0.0979	0.0039	0.0064	0.0002	0.0064
0.90	0.27	−0.0879	0.0035	0.0078	0.0006	0.0078
0.34	0.38	−0.0219	0.0100	0.0202	0.0108	0.0170
0.50	0.43	−0.0759	0.0032	0.0055	0.0008	0.0052
0.69	0.44	−0.1271	0.0038	0.0063	0.0012	0.0059
0.89	0.43	−0.1182	0.0054	0.0100	0.0002	0.0098
0.54	0.58	−0.1211	0.0108	0.0160	0.0016	0.0159
0.70	0.64	−0.1474	0.0049	0.0075	0.0003	0.0075
0.89	0.67	−0.1612	0.0059	0.0107	0.0022	0.0105

observed for higher p_T. In Ref. [7], spin effects by the absorptive corrections, which are initial/final-state interactions, start to increase from $p_T \sim 0.2$ GeV/c. However, it is also expected in that calculation that the absolute value of the neutron A_N is larger in $0.40 < x_F < 0.60$ than that in $0.60 < x_F < 1.00$, which is opposite to the measurements. Other Regge poles like ρ and a_2 may enhance the asymmetry in $0.60 < x_F < 1.00$, because the spin effect by the ρ and a_2 exchange can also have a finite contribution compared to the π and a_1 exchange in the higher-x_F region [25]. More comprehensive theoretical considerations are necessary to understand the x_F dependence in $p_T > 0.3$ GeV/c. Thus far, no Reggeon exchange model and absorptive corrections can explain the x_F dependence in $p_T < 0.3$ GeV/c; therefore, more precise theoretical calculations, or the inclusion of new processes other than the above production mechanism may be necessary to explain the present results.

VI. SUMMARY

The RHICf Collaboration installed the RHICf detector at the zero-degree area of the STAR detector and measured the A_N for forward neutron production in polarized $p + p$ collisions at $\sqrt{s} = 510$ GeV. This measurement covered a wide p_T range with high resolution to help us better understand the production mechanism for forward neutrons. The resulting A_N increases in magnitude with p_T in the high-x_F range, but it reaches a plateau in the low-x_F range. There are indications that the asymmetries also level off at high x_F, but the magnitude increases with increasing p_T bins. No $\sqrt{s}$ dependence was observed when the RHICf data were compared with PHENIX. The existing theoretical calculation based on the π and a_1 exchange between two protons reproduced only part of the data. To understand the present results, some additional spin effects beyond the π and a_1 exchange scenario will be necessary.

ACKNOWLEDGMENTS

We thank the staff of the Collider-Accelerator Department at Brookhaven National Laboratory, the STAR Collaboration, and the PHENIX Collaboration for supporting the experiment. We especially acknowledge the essential supports from the STAR members for the design and the construction of the detector manipulator, the installation/uninstallation, the integration of the data acquisition system, and the operation and management of all these collaborative activities. This work was supported by the U.S.-Japan Science and Technology Cooperation Program in High Energy Physics, JSPS KAKENHI (Grants No. JP26247037, No. JP18H01227, and No. JP21H04484), the joint research program of the Institute for Cosmic Ray Research (ICRR), University of Tokyo, the NRF grants for the Center for Extreme Nuclear Matters (CENuM) funded by MSIT of Korea (Grant No. 2018R1A5A1025563), and the "UNICT" program, University of Catania.

[1] Y. Fukao *et al.*, Single transverse-spin asymmetry in very forward and very backward neutral particle production for polarized proton collisions at $\sqrt{s} = 200$ GeV, Phys. Lett. B **650**, 325 (2007).

[2] K. Tanida (PHENIX Collaboration), Energy and transverse momentum dependence of single-spin asymmetry of very forward neutron in polarized pp collision, J. Phys. Conf. Ser. **295**, 012097 (2011).

[3] J. Soffer and N. A. Törnqvist, Origin of the polarization for inclusive Λ production in pp collisions, Phys. Rev. Lett. **68**, 907 (1992).

[4] U. D'Alesio and H. J. Pirner, Target fragmentation in pp, ep and γp collisions at high energies, Eur. Phys. J. A **7**, 109 (2000).

[5] B. Z. Kopeliovich, B. Povh, and I. K. Potashnikova, Deep-inelastic electroproduction of neutrons in the proton fragmentation region, Z. Phys. C **73**, 125 (1996).

[6] W. Flauger and F. Mönnig, Measurement of inclusive zero-angle neutron spectra at the CERN ISR, Nucl. Phys. **B109**, 347 (1976).

[7] B. Z. Kopeliovich, I. K. Potashnikova, and Iván Schmidt, and J. Soffer, Single transverse spin asymmetry of forward neutrons, Phys. Rev. D **84**, 114012 (2011).

[8] U. A. Acharya *et al.* (PHENIX Collaboration), Transverse single spin asymmetries of forward neutrons in $p + p$, $p + \mathrm{Al}$, and $p + \mathrm{Au}$ collisions at $\sqrt{s_{NN}} = 200$ GeV as a function of transverse and longitudinal momenta, Phys. Rev. D **105**, 032004 (2022).

[9] C. Adler, A. Denisov, E. Garcia, M. Murray, H. Stroebele, and S. White, The RHIC zero degree calorimeters, Nucl. Instrum. Methods Phys. Res., Sect. A **470**, 488 (2001).

[10] O. Adriani *et al.* (LHCf Collaboration), Measurements of longitudinal and transverse momentum distributions for neutral pions in the forward-rapidity region with the LHCf detector, Phys. Rev. D **94**, 032007 (2016).

[11] RHICf Collaboration, Performance of RHICf detector during operation in 2017, J. Instrum. **16**, P10027 (2021).

[12] M. H. Kim *et al.* (RHICf Collaboration), Transverse single-spin asymmetry for very forward neutral pion production in polarized $p + p$ collisions at $\sqrt{s} = 510$ GeV, Phys. Rev. Lett. **124**, 252501 (2020).

[13] S. Ostapchenko, Monte Carlo treatment of hadronic interactions in enhanced Pomeron scheme: QGSJET-II model, Phys. Rev. D **83**, 014018 (2011).

[14] S. Agostinelli *et al.*, GEANT4: A simulation toolkit, Nucl. Instrum. Methods Phys. Res., Sect. A **506**, 250 (2003).

[15] O. Adriani *et al.* (LHCf Collaboration), Measurement of zero degree single photon energy spectra for $\sqrt{s} = 7$ TeV proton-proton collisions at LHC, Phys. Lett. B **703**, 128 (2011).

[16] K. Kawade *et al.*, The performance of the LHCf detector for hadronic showers, J. Instrum. **9**, P03016 (2014).

[17] Y. Makino *et al.*, Performance study for the photon measurements of the upgraded LHCf calorimeters with Gd_2SiO_5 (GSO) scintillators, J. Instrum. **12**, P03023 (2017).

[18] O. Jinnouchi *et al.*, Results from the RHIC PC CNI Polarimeter for 2003, RHIC/CAD Accelerator Physics Note 171 (2004).

[19] H. Okada *et al.*, Measurement of the analyzing power A_N in pp elastic scattering in the CNI region with a polarize atomic hydrogen gas jet target, Phys. Lett. B **638**, 450 (2006).

[20] C. A. Whitten, Jr. *et al.* (STAR Collaboration), The Beam-Beam Counter: A Local Polarimeter at STAR, https://www.star.bnl.gov/~eca/LocalPol/BBCproceeding-Chuck.pdf.

[21] W. J. Llope *et al.*, The STAR vertex position detector, Nucl. Instrum. Methods Phys. Res., Sect. A **759**, 23 (2014).

[22] G. D'Agostini, A multidimensional unfolding method based on Bayes' theorem, Nucl. Instrum. Methods Phys. Res., Sect. A **362**, 487 (1995).

[23] T. Adye, Unfolding algorithms and tests using RooUnfold, in *PHYSTAT 2011* (CERN, Geneva, 2011), p. 313, arXiv:1105.1160.

[24] R. Brun and F. Rademakers, ROOT: An object oriented data analysis framework, Nucl. Instrum. Methods Phys. Res., Sect. A **389**, 81 (1997).

[25] G. Mitsuka, Private discussion based on [7] (2023).